Simultaneous improvement of martensitic phase transition and ductility in Cu-doped and/or alloyed all-*d*-metal Ni_2MnTa Heusler compounds

Guijiang Li[1,*], Lei Xu[1], Zhenhua Cao[1]

[1]College of Materials Science and Engineering, Nanjing Tech University, Nanjing 211816, China

Supplementary materials

A. The calculation details for elastic related parameters

The cubic all-*d*-metal Heusler compounds possess three independent elastic constants, i.e., C_{11}, C_{12}, and C_{44}. Among them, the C_{11} and C_{12} were obtained from the tetragonal shear modulus $C' = (C_{11} - C_{12})/2$ and the bulk modulus $B = (C_{11} + 2C_{12})/3$ [1]. Herein, the equilibrium volume and bulk modulus were determined by fitting the calculated total energy versus volume to a Morse function[2]. The tetragonal shear modulus C' and the cubic elastic modulus C_{44} were derived from the volume-conserving orthorhombic deformation and monoclinic deformation. By fitting the total energies with respect to adopted orthorhombic (δ_o) and monoclinic (δ_m) distortions as $E(\delta_o) = E(0) + 2VC'\delta_o^2$ and $E(\delta_m) = E(0) + 2VC_{44}\delta_m^2$, both C' and C_{44} can be obtained. These methods allow for the determination of the C_{11}, C_{12} and C_{44}. The elastic moduli in this study are calculated by following Voigt–Reuss–Hill (VRH) approximation[3-5]. By Voigt and Reuss approximations, the bulk and shear moduli can be derived by $B_V = B_R = \frac{C_{11} + 2C_{12}}{3}$, $G_V = \frac{(C_{11} - C_{12} + 3C_{44})}{5}$ and $G_R = \frac{5(C_{11} - C_{12})C_{44}}{4C_{44} + 3(C_{11} - C_{12})}$. Then, average bulk and shear moduli ($B_H = \frac{B_V + B_R}{2}$ and $G_H = \frac{G_V + G_R}{2}$) was calculated by adopting the VRH approximation. Furthermore, Poisson's ratio was deduced by $\nu = \frac{3B - 2G}{2(3B + G)}$ [1]. The Debye temperature (Θ_D) can be obtained from the average sound velocity based on the equation of $\Theta_D = \frac{h}{k_B}\left[\frac{3q}{4\pi}\frac{N_A\rho}{M}\right]^{1/3} v_m$ [6]. Herein, h and K_B are the Planck and Boltzmann constants, q is the number of atoms in each formula unit, N_A is the Avogadro's number,

* Corresponding author (email: guijiangli@njtech.edu.cn)

M is the molecular weight per formula unit, ρ is the density. V_m ($v_m = \left[\frac{1}{3}\left(\frac{2}{v_t^3}+\frac{1}{v_l^3}\right)\right]^{-1/3}$) is the average velocity, where v_l ($=\sqrt{\left(B+\frac{4}{3}G\right)\frac{1}{\rho}}$) and v_t ($=\sqrt{\frac{G}{\rho}}$) are longitudinal and transverse sound velocities, respectively. The Cauchy's pressure in this study for all-d-metal Heusler compounds was defined by the Cauchy relation as $C_{12}-C_{44}$ [1].

B. Atomic preferential occupation in Cu-doped and/or alloyed Ni_2MnTa

In $L2_1$-type Ni_2MnTa at ground state, the two Ni atoms occupy 8c sites. Ta and Mn atoms lie in 4a and 4b sites, respectively. To obtain the stable cubic structure, the preferential atomic occupation styles in $Ni_{2-x}Cu_xMnTa$, $Ni_2Mn_{1-x}Cu_xTa$, and $Ni_2MnTa_{1-x}Cu_x$ alloys were first investigated. For each of the three alloys series, five possible atomic occupation styles were considered herein. Considering $Ni_{2-x}Cu_xMnTa$ as representative example, the considered atomic occupation styles are as follows: (I) the newly introduced Cu atoms directly occupy Ni sub-lattices, (II) Cu atoms occupy Mn sub-lattices and original Mn atoms are forced to move to Ni sub-lattices. (III) Cu atoms occupy Ta sub-lattices and original Ta atoms are forced to move to Ni sub-lattices. (IV) Cu atoms occupy Mn sub-lattices, original Mn atoms are forced to move to Ta sub-lattices, and Ta atoms then move to Ni sub-lattices. (V) Cu atoms occupy Ta sub-lattices, and original Ta atoms are forced to move to Mn sub-lattices, and Mn atoms then move to Ni sub-lattices. Based on above-mentioned atomic configurations in these series of alloys, the calculated energy listed in Table SI indicates that newly introduced Cu atoms prefer to direct atomic occupation style in $Ni_{2-x}Cu_xMnTa$, $Ni_2Mn_{1-x}Cu_xTa$, as described in style (I). For $Ni_2MnTa_{1-x}Cu_x$ alloys, the introduced Cu atoms prefer to occupy the Mn sub-lattice, and original Mn atoms are forced to move to Ta sub-lattices, as described in style (III). In Heusler alloys, the empirical atomic occupation rule indicates that transition metal atoms with more valence electrons prefer to occupy 8c sites. However, those with less valence electrons occupy 4a and/or 4b sites[7]. In Cu-doped and/or alloyed Ni_2MnTa alloys, Cu atom possesses the most valence electrons. Thus, following this empirical atomic occupation rule, Cu atoms then preferentially occupy 8c sites. Theoretically, atomic occupation only in $Ni_{2-x}Cu_xMnTa$ alloys agrees well with conventional rule. Atomic occupations in $Ni_2Mn_{1-x}Cu_xTa$ and $Ni_2MnTa_{1-x}Cu_x$ alloys exhibit abnormal behaviors. Herein, atomic occupation styles in $Ni_{2-x}Cu_xMnTa$, $Ni_2Mn_{1-x}Cu_xTa$ are same as the case in Cu-doped and/or alloyed Ni_2MnGa[8, 9]. In Heusler alloys, high-ordered atomic occupations are dominated by strong interatomic covalent hybridization strength[10-12]. When the covalent hybridization level decreases, abnormal atomic occupation can occur [11]. In $Ni_2Mn_{1-x}Cu_xTa$ and $Ni_2MnTa_{1-x}Cu_x$ alloys, the abnormal atomic occupation indicates the weakening of the covalent hybridization strength dependence of Cu content. The preferential atomic occupation in $Ni_{2-x}Cu_xMnTa$ alloys indicates that the covalent hybridization level remains at a higher level or decrease slightly. The

future experiments such as high-resolution neutron diffractions can help to identify the atomic occupation in $Ni_2Mn_{1-x}Cu_xTa$ and $Ni_2MnTa_{1-x}Cu_x$ alloys.

Table SI. Different atomic occupation styles in Cu-doped and/or alloyed Ni_2MnTa alloys. Considering the energy of atomic occupation style I as reference, the relative energy difference (ΔE in mRy) was obtained to determine the stable atomic occupation.

	Composition	Atomic occupation	ΔE
$Ni_{2-x}Cu_xMnTa$ x=0.1	I. $Ni_{2-x}Cu_xMnTa$	0	
	II. $(Ni_{2-x}Mn_x)(Mn_{1-x}Cu_x)Ta$	1.30	
	III. $(Ni_{2-x}Ta_x)Mn(Ta_{1-x}Cu_x)$	78.02	
	IV. $(Ni_{2-x}Ta_x)(Mn_{1-x}Cu_x)(Ta_{1-x}Mn_x)$	529.78	
	V. $(Ni_{2-x}Mn_x)(Mn_{1-x}Ta_x)(Ta_{1-x}Cu_x)$	32.36	
$Ni_2(Mn_{1-x}Cu_x)Ta$ x=0.01	I. $Ni_2(Mn_{1-x}Cu_x)Ta$	0	
	II. $(Ni_{2-x}Cu_x)(Mn_{1-x}Ni_x)Ta$	0.38	
	III. $Ni_2(Mn_{1-x}Ta_x)(Ta_{1-x}Cu_x)$	121.90	
	IV. $(Ni_{2-x}Cu_x)(Mn_{1-x}Ta_x)(Ta_{1-x}Ni_x)$	122.30	
	V. $(Ni_{2-x}Ta_x)(Mn_{1-x}Ni_x)(Ta_{1-x}Cu_x)$	152.62	
$Ni_2Mn(Ta_{1-x}Cu_x)$ x=0.01	I. $Ni_2Mn(Ta_{1-x}Cu_x)$	0	
	II. $(Ni_{2-x}Cu_x)Mn(Ta_{1-x}Ni_x)$	0.38	
	III. $Ni_2(Mn_{1-x}Cu_x)(Ta_{1-x}Mn_x)$	-1.07	
	IV. $(Ni_{2-x}Cu_x)(Mn_{1-x}Ni_x)(Ta_{1-x}Mn_x)$	-0.69	
	V. $(Ni_{2-x}Mn_x)(Mn_{1-x}Cu_x)(Ta_{1-x}Ni_x)$	0.50	

C. Lattice sizes in Cu-doped and/or alloyed Ni_2MnTa

Based on stable atomic occupation styles in $Ni_{2-x}Cu_xMnTa$, $Ni_2Mn_{1-x}Cu_xTa$, and $Ni_2MnTa_{1-x}Cu_x$ alloys, the lattice parameters of cubic phase were obtained by geometry optimization, as presented in Fig. S1. Theoretically, the lattice sizes of cubic phase in both $Ni_{2-x}Cu_xMnTa$, $Ni_2Mn_{1-x}Cu_xTa$, and $Ni_2MnTa_{1-x}Cu_x$ alloys all decreased with the doping of Ni, Mn and Ta atoms by Cu atoms. In Cu-doped and/or alloyed all-*d*-metal Heusler compounds Ni_2MnTa, the metallic bonding becomes prevalent, which is different from conventional p-d covalent hybridization dominated Ni-Mn-based Heusler compounds. Owing to the volume effect of metallic bonding, materials tend to crystallize in relatively close packed structures. The closer the arrangement of atoms, the lower the Coulomb energy and the more stable the binding. Thus, the increased metallic bonding in $Ni_{2-x}Cu_xMnTa$, $Ni_2Mn_{1-x}Cu_xTa$, and $Ni_2MnTa_{1-x}Cu_x$ alloys alloys resulted in the contraction of lattice sizes.

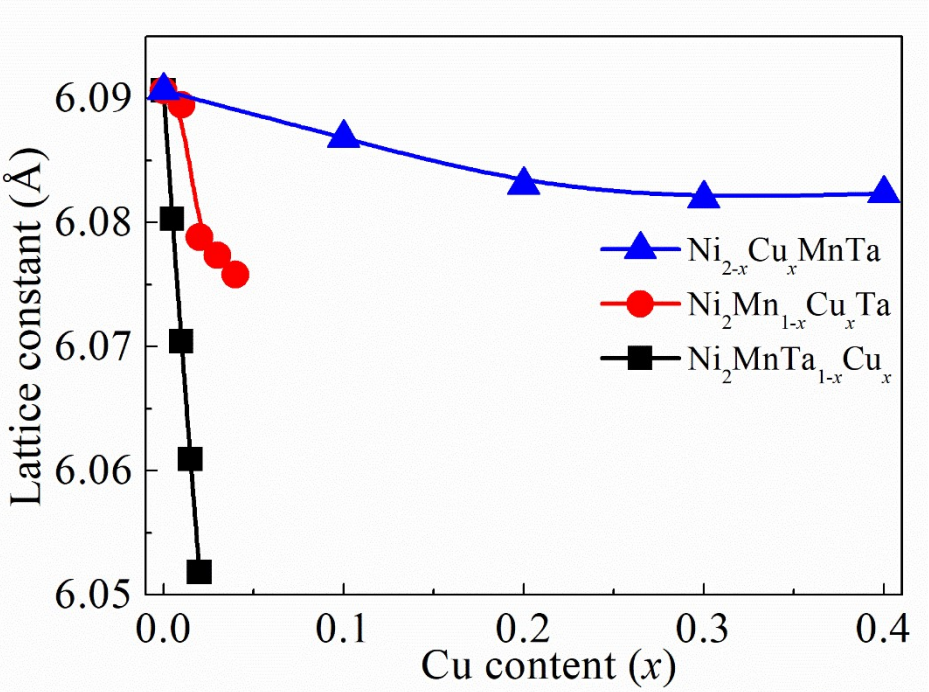

FIG. S1 Lattice parameters of (a) $Ni_{2-x}Cu_xMnTa$, (b) $Ni_2Mn_{1-x}Cu_xTa$, and (c) $Ni_2MnTa_{1-x}Cu_x$ alloys.

D. Magnetic moments in Cu-doped and/or alloyed Ni_2MnTa

Based on theoretical atomic occupation styles and optimized lattice parameters, the magnetic moments were calculated in Cu-doped and/or alloyed Ni_2MnTa and shown in Table SII.

Table SII. The calculated magnetic moments (in μ_B/f.u.), as well as the calculated atomic magnetic moments (in μ_B/atom) for $Ni_{2-x}Cu_xMnTa$, $Ni_2Mn_{1-x}Cu_xTa$, and $Ni_2MnTa_{1-x}Cu_x$ alloys with varying compositions.

Composition	Ni(*A*,*C*)	Cu(*A*,*C*)	Mn(*B*)	Cu(*B*)	Ta(*D*)	Mn(*D*)	Total
Ni_2MnTa	0.29		3.64		-0.031		4.19
$Ni_{1.9}Cu_{0.1}MnTa$	0.29	0.030	3.62		-0.035		4.15
$Ni_{1.8}Cu_{0.2}MnTa$	0.30	0.028	3.62		-0.038		4.13
$Ni_{1.7}Cu_{0.3}MnTa$	0.31	0.026	3.61		-0.040		4.11
$Ni_{1.6}Cu_{0.4}MnTa$	0.32	0.024	3.61		-0.044		4.10
$Ni_2Mn_{0.99}Cu_{0.01}Ta$	0.29		3.64	0.007	-0.030		4.15
$Ni_2Mn_{0.98}Cu_{0.02}Ta$	0.28		3.62	0.015	-0.030		4.09
$Ni_2Mn_{0.97}Cu_{0.03}Ta$	0.28		3.62	0.016	-0.030		4.04
$Ni_2Mn_{0.96}Cu_{0.04}Ta$	0.28		3.61	0.016	-0.030		4.00
$Ni_2MnTa_{0.99}Cu_{0.01}$	0.28		3.61	0.015	-0.034	-4.02	4.06
$Ni_2MnTa_{0.98}Cu_{0.02}$	0.27		3.59	0.015	-0.037	-4.00	3.95
$Ni_2MnTa_{0.97}Cu_{0.03}$	0.27		3.57	0.015	-0.039	-3.98	3.84
$Ni_2MnTa_{0.96}Cu_{0.04}$	0.26		3.55	0.016	-0.041	-3.97	3.73

E. The electron density difference (EDD) distribution of Cu-doped and/or alloyed Ni_2MnTa

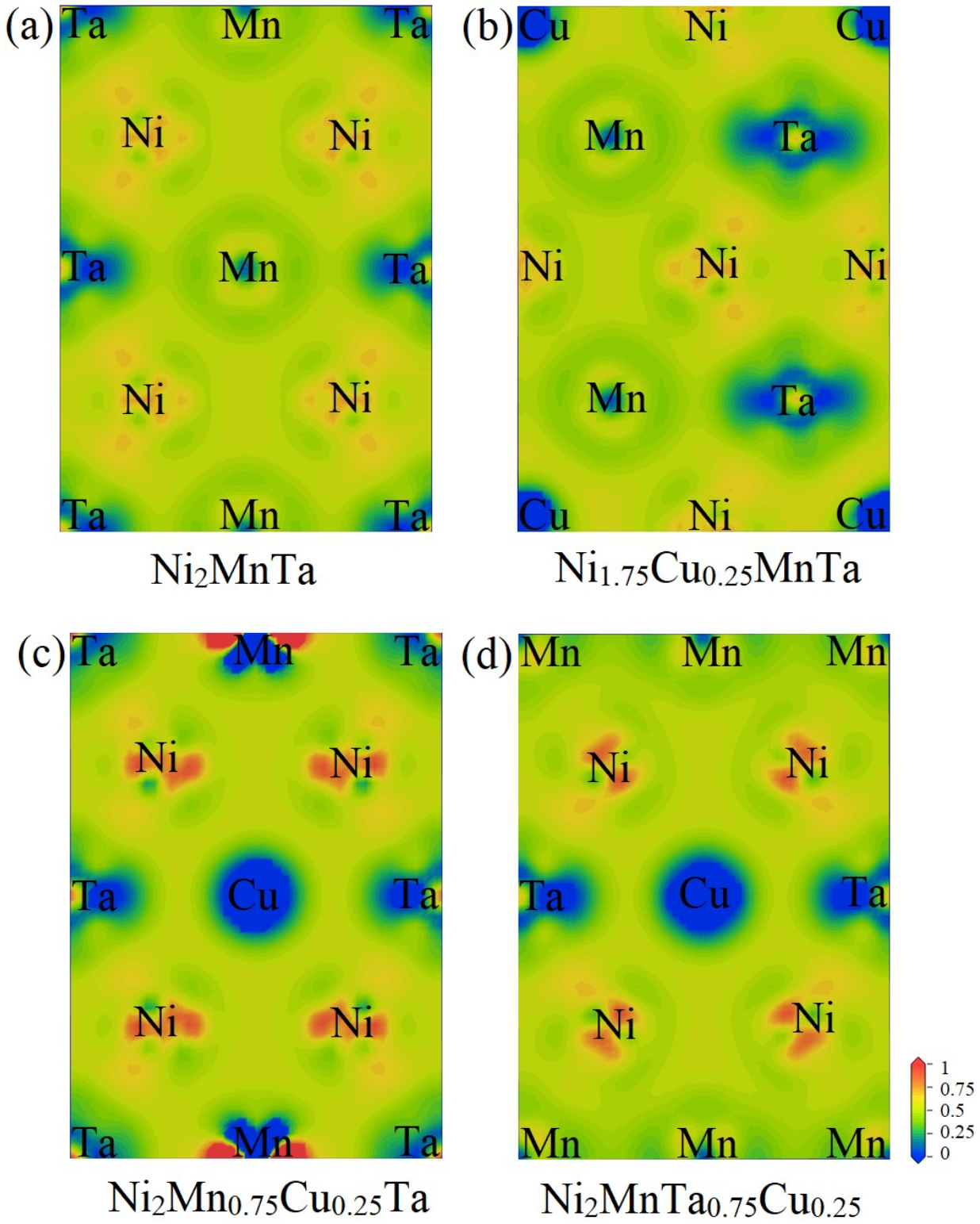

Fig. SII EDD maps for (a) Ni_2MnTa, (b) $Ni_{1.75}Cu_{0.25}MnTa$, (c) $Ni_2Mn_{0.75}Cu_{0.25}Ta$, and (d) $Ni_2MnTa_{0.75}Cu_{0.25}$ on (110) plane in cubic unit cells. On the lower right corner, there is a reference bar for EDD value. The comparison of these maps aids in revealing changes in interatomic hybridization.

Reference

1. *L. Vitos, Computational Quantum Mechanics for Materials Engineers: The EMTO Method and Applications (Springer-Verlag, London, 2007).*
2. V. L. Moruzzi, J. F. Janak and K. Schwarz, *Phys. Rev. B*, 1988, **37**, 790-799.
3. A. Reuss, *Z. Ang. Math. Mech.* , 1929, **9**, 49-58.
4. R. Hill, *Proc. Phys. Soc. Sect. A*, 1952, **65**, 349-354.
5. W. Voigt, *Ann. Phys.* , 1889, **274**, 573-587.
6. O. L. Anderson, *J. Phys. Chem. Solids* 1963, **24**, 909-917.
7. T. J. Burch, T. Litrenta and J. I. Budnick, *Phys. Rev. Lett.*, 1974, **33**, 421-424.
8. A. Chakrabarti, M. Siewert, T. Roy, K. Mondal, A. Banerjee, M. E. Gruner and P. Entel, *Phys. Rev. B*, 2013, **88**, 174116.
9. C. M. Li, H. B. Luo, Q. M. Hu, R. Yang, B. Johansson and L. Vitos, *Phys. Rev. B*, 2011, **84**, 024206.
10. G. J. Li, E. K. Liu, H. G. Zhang, J. F. Qian, H. W. Zhang, J. L. Chen, W. H. Wang and G. H. Wu, *Appl. Phys. Lett.*, 2012, **101**, 102402-102404.
11. G. J. Li, E. K. Liu, H. G. Zhang, Y. J. Zhang, G. Z. Xu, H. Z. Luo, H. W. Zhang, W. H. Wang and G. H. Wu, *Appl. Phys. Lett.*, 2013, **102**, 062407.
12. G. J. Li, E. K. Liu, Y. J. Zhang, Y. Du, H. W. Zhang, W. H. Wang and G. H. Wu, *J. Appl. Phys.*, 2013, **113**, 103903.